# Supporting Information: Planar chirality and optical spin-orbit coupling for chiral Fabry-Perot cavities

Jérôme Gautier, Minghao Li, Thomas W. Ebbesen, and Cyriaque Genet*

*Université de Strasbourg, CNRS, Institut de Science et d'Ingénierie Supramoléculaires, UMR 7006, F-67000 Strasbourg, France*

E-mail: genet@unistra.fr

## 1 Sample fabrication

The fabrication process for our cavities is simple. We first thoroughly clean a $2.5 \times 2.5$ $cm^2$ glass substrate by sonication in a 0.5%wt Hellmanex solution in ultra-pure water for 8 minutes. We then sonicate the substrate in a bath of ultra-pure water only, for 30 minutes followed by a sonicated bath in pure ethanol for 30 other minutes. We finally rinse the substrate using a series of 20 dips in a solution of ultra-pure water.

In order to form the cavity itself, we first sputter a layer of silver using an Emitech K575X tabletop sputterer at 60 mA (for 45 s for 30 nm and 95 s for 60 nm Ag layers). On top of the Ag mirror thus sputtered, we spin-coat a solution of dissolved Polystyrene,4%wt in Toluene at 1400 RPM for 2 min to obtain a thin film of 150 nm. The RPM speed was calibrated using profilometry. We finally "close" the cavity by sputtering another Ag layer on top, using the same sputter parameters for the same thickness.

## 2 Experimental setup

Our experimental setup used for the full determination of the Mueller matrix (MM) element is schematized in S1. The first part is made of a polarization state generator (PSG) composed of a Glan-Taylor (GT) linear polarizer and a motorized quarter-wave plate. The light beam is injected through the sample using a Nikon ELWD 40× (NA=0.6) objective and collected using a Nikon ELWD 100× (NA=0.9) objective. The collected light passes through a polarization state analyzer (PSA) composed of a quarter-wave plate and a linear polarizer (LP). The two linear polarizers were chosen different because of the negative bias induced on the MM elements when using a GT within the PSA. The last part is made of a lens set at the focal distance from the back focal plane (BFP) of the second objective, associated with a second lens at the entry of a spectrometer (Teledyne Princeton Instrument, SpectraPro HRS-300) for imaging this BFP –referred below as "Fourier space imaging". Removing this lens gives us the ability to image the focal plane of the objective on the CCD –referred as "real space imaging". Spatially resolved, the spectra are recorded using a PIXIS 1024 CCD camera.

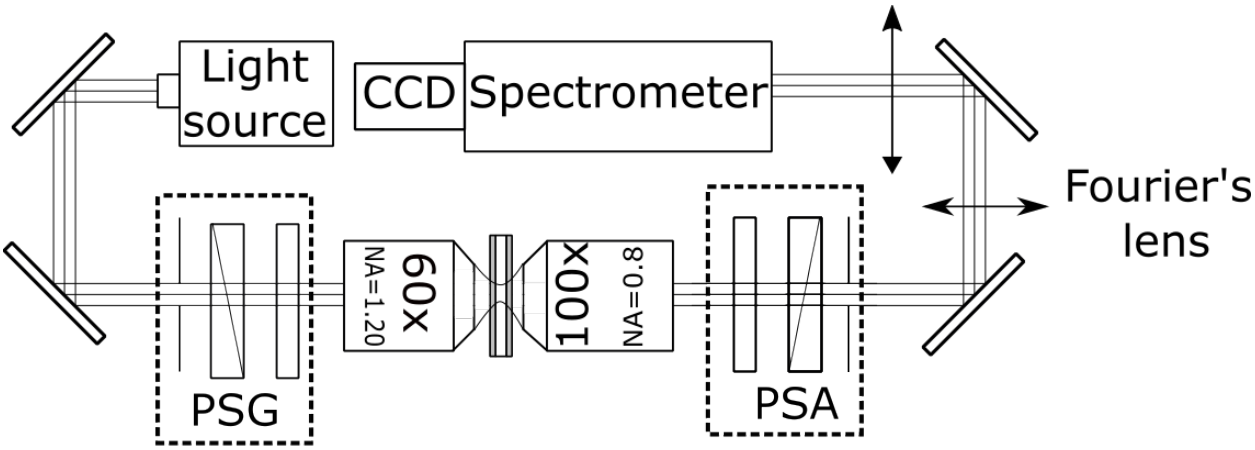


Figure S1: Experimental setup used for the Muller matrix determination, composed of a polarization state generator (PSG) and analyzer (PSA). The two lenses give us the ability to image the BFP of the objective, i.e. the Fourier space of our sample.

In order to resolve the MM for a given wavelength, we build a system of equation linking

the measured intensity for a given state of polarization (SOP) to its MM element. The SOP are generated using a carefully chosen combination of angles for the quarter waveplates in both the PSA and PSG.

Because the MM is a $4 \times 4$ matrix, there are at least 16 linearly independent equations to solve for our system. Experimentally, we overestimate this minimal set by doing 64 measurements, solving the system by the least-square method. This approach was already detailed by us in[S1] and is simply summarized here.

Let $\boldsymbol{M_S}$, $\boldsymbol{M_{PSA}}$, $\boldsymbol{M_{PSG}}$ be the MM of the sample, the PSA, and respectively the PSG. We can form the following system of equations represented in the following matrix form:

$$\mathbf{S}_{\text{out}} = \boldsymbol{M}_{\text{PSA}} \boldsymbol{M}_{\text{S}} \boldsymbol{M}_{\text{PSG}} \mathbf{S}_{\text{in}} \tag{1}$$

The intensity recorded, for one experiment, by the CCD, corresponds to the first element of $\mathbf{S}_{\text{out}}$ , $I_{\text{out}}$, which can be expressed as:

$$I_{\text{out}} = \sum_{j=1}^{4} \sum_{i=1}^{4} m_{1,i}^{\text{PSA}} \times g_i \times m_{j-1,i}^{\text{S}} \tag{2}$$

where $m_{1,i}^{\text{PSA}}$ is the known first line of the PSA MM element, $g_i$ the known element of the vector resulting from $\boldsymbol{M_{PSG}} \cdot \mathbf{S}_{\text{in}}$, and $m_{j,i}^{\text{S}}$ the unknown MM element of the sample. We write our set of 64 equations linking the intensity and the MM element in the following and most convenient matrix formulation:

$$\mathbf{b}_{64\times1} = \boldsymbol{A}_{64\times16} \cdot \mathbf{X}_{16\times1} \tag{3}$$

where $\mathbf{b}$ is a containing each intensity of the 64 measurement, and $\mathbf{X}$ is a vector containing all the MM elements. Because we overestimate our system, there is no unique solution but

there is a unique solution that minimize the residue $\nu^2$:

$$\nu^2 = (\mathbf{b} - \boldsymbol{A}.\mathbf{X})^T.(\mathbf{b} - \boldsymbol{A}.\mathbf{X}) \tag{4}$$

The vector that minimize the residue can be expressed as:

$$\mathbf{X} = (\boldsymbol{A}^T\boldsymbol{A})^{-1}\boldsymbol{A}^T\mathbf{b}. \tag{5}$$

From eq (5), one can uniquely define the MM associated with the change of the incident light SOP through the medium. Alone however, the Muller matrix is hardly useful in a chiroptical context. In order to access genuine chiroptical observables, some data filtering is necessary in order to remove any optical artifacts that would prevent us from recovering the relevant chiroptical features of the sample, in particular its circular dichroism.

# 3 Data filtering

From an experimental MM, one can develop an algebra, which allows to isolate the CD signal of the sample and remove artifact signals in the system. This well-known algebra is detailed for instance in.[S2] For our experiments, two different data filtering steps were used when imaging real space vs. Fourier space.

In the real space, we first identify the polarization responses of the objectives by measuring the MM of $(i)$ a setup with two $\boldsymbol{M}_{40\times}$ and no sample, and $(ii)$ of the setup described in S1. We find indeed that experimentally, $\boldsymbol{M}_{40\times} \simeq \boldsymbol{M}_{100\times}$. One can then remove the response of the objective by noting that when measuring an empty setup, i.e. with no sample, one effectively measures:

$$\boldsymbol{M}_{\text{empty}} = \boldsymbol{M}_{40\times}\boldsymbol{M}_{40\times} \tag{6}$$

$$\tag{7}$$

We can then compute $\boldsymbol{M}_{40\times} = (\boldsymbol{M}_{\text{empty}})^{\frac{1}{2}}$ and remove the responses of our objectives in the real space. In Fourier space the same procedure is applied.

The second filtering step consists in removing the contribution of the glass substrate of the sample from our experimental MM. To do so, we first measure the response in both real and Fourier spaces of the cleaned substrate, $\boldsymbol{M}_{glass}$. Then, we can determine the MM of the sample alone without the glass substrate contributions by using the following serial MM decomposition:

$$\boldsymbol{M}_{\text{S}} = \boldsymbol{M}_{\text{glass}}\boldsymbol{M}_{\text{FP}} \tag{8}$$

where $\boldsymbol{M}_{\text{FP}}$ is the MM of the Fabry-Perot cavity (without substrate) which can be rewritten as $\boldsymbol{M}_{\text{FP}} = \boldsymbol{M}_{\text{glass}}^{-1}\boldsymbol{M}_{\text{S}}$.

The third filtering step is to decompose the previously obtained MM using the Cloude decomposition.[S3] The goal of the method is to give an estimation of the equivalent non-depolarizing MM, known as Mueller-Jones matrix, necessary for the last filtering step below. Following,[S2,S4] Cloude decomposition consists in computing the $4 \times 4$ hermitian coherency

matrix $\boldsymbol{T}$, which will have the following matrix elements:

$$
\begin{aligned}
t_{11} &= \frac{1}{4}(m_{00} + m_{11} + m_{22} + m_{33}) \\
t_{12} &= \frac{1}{4}(m_{01} + m_{10} - i(m_{23} - m_{32})) \\
t_{13} &= \frac{1}{4}(m_{02} + m_{20} - i(m_{31} - m_{13})) \\
t_{14} &= \frac{1}{4}(m_{03} + m_{30} - i(m_{12} - m_{21})) \\
t_{22} &= \frac{1}{4}(m_{00} + m_{11} - m_{22} - m_{33}) \\
t_{23} &= \frac{1}{4}(m_{12} + m_{21} - i(m_{30} - m_{03})) \\
t_{24} &= \frac{1}{4}(m_{13} + m_{13} - i(m_{02} - m_{20}) \\
t_{33} &= \frac{1}{4}(m_{00} - m_{11} + m_{22} - m_{33}) \\
t_{34} &= \frac{1}{4}(m_{23} + m_{32} - i(m_{10} - m_{01})) \\
t_{44} &= \frac{1}{4}(m_{00} - m_{11} - m_{22} + m_{33})
\end{aligned}
$$

The coherency matrix can be computed from any given experimental matrix. By considering that any depolarizing MM can be considered as a convex sum of non-depolarizing Mueller-Jones matrix, denoted $\boldsymbol{M}_{Ji}$, one can link the eigenvalues $\lambda_i$ of the coherency matrix to $\boldsymbol{M}_S$ by the following:

$$\boldsymbol{M} = \sum_{i=0}^{3} \lambda_i \boldsymbol{M}_{Ji} \tag{9}$$

$$\boldsymbol{M}_{Ji} = \boldsymbol{A}(\boldsymbol{J_i} \otimes \boldsymbol{J_i^*})\boldsymbol{A}^{-1} \tag{10}$$

where $\boldsymbol{J}_i$ is the Mueller-Jones matrix associated to $\boldsymbol{M}_{Ji}$ and $\boldsymbol{A}$ is the passage matrix that

can be written as

$$\boldsymbol{A} = \begin{pmatrix} 1 & 0 & 0 & 1 \\ 1 & 0 & 0 & -1 \\ 0 & 1 & 1 & 0 \\ 0 & -i & i & 0 \end{pmatrix} \tag{11}$$

We then can rank the $\boldsymbol{M}_{Ji}$ in terms of their respective weight. Generally, this decomposition is dominated by the first term, ie $\lambda_0 >> \lambda_1, \lambda_2, \lambda_3$, and one can consider $\lambda_0 \boldsymbol{M}_{J0}$ as a good estimate of the non-depolarizing Muller matrix associated to $\boldsymbol{M}_S$. From this estimate, one can directly extract the CD following.[S5] We first compute the cumulated differential MM $\boldsymbol{L}_m$ as

$$\boldsymbol{L}_m = \ln(\boldsymbol{M}_{\mathrm{J0}}) \tag{12}$$

$$= \frac{1}{2}(\boldsymbol{L} - \boldsymbol{G}\boldsymbol{L}^T\boldsymbol{G}) \tag{13}$$

where $\boldsymbol{G}$ is the Minkowski tensor $\boldsymbol{G}$=diag(1,-1,-1,-1) and ln the matrix logarithm. In this manner, the CD simply corresponds to the $\boldsymbol{L}_m(0,3)$ matrix element.

# 4 Bi-signated CD signals for $TE$ and $TM$ modes

In order to explain the bi-signated CD signal for the $TE$ and $TM$ modes measured through the cavity under oblique illumination, we look at the helicity of the transmitted beam under $TE$ and $TM$ polarizations at normal incidence, where the two associated modes are degenerated. Within the Stokes-Mueller formalism, $TE$ and $TM$ modes are expressed by Stokes vectors as $\mathbf{S}_{TM} = (1, -1, 0, 0)^T$ and $\mathbf{S}_{TE} = (1, 1, 0, 0)^T$. Since our system at normal

incidence is a 2D chiral system, it is simply described by a Jones-Mueller matrix given by

$$\boldsymbol{M}_{2D} = \begin{pmatrix} 1 & -a_1 & -a_2 & 0 \\ -a_1 & d_1 & 0 & b_2 \\ -a_2 & 0 & d_2 & -b_1 \\ 0 & -b_2 & b_1 & d_3 \end{pmatrix}, \tag{14}$$

and therefore yielding the TE and TM transmitted Stokes vectors:

$$\mathbf{S}_{TM}^{\text{out}} = \boldsymbol{M}_{2D} \cdot \mathbf{S}_{TM} = \begin{pmatrix} 1 + a_1 \\ -a_1 - \alpha \\ -a_2 \\ b_2 \end{pmatrix} \tag{15}$$

$$\mathbf{S}_{TE}^{\text{out}} = \boldsymbol{M}_{2D} \cdot \mathbf{S}_{TE} = \begin{pmatrix} 1 - a_1 \\ -a_1 + \alpha \\ -a_2 \\ -b_2 \end{pmatrix}. \tag{16}$$

The $S_3$ elements $\pm b_2$ for each transmitted Stokes vector are opposite. This implies that the helicities associated with the $TE$ and $TM$ modes, degenerated at normal incidence, are opposite. When the optical activity emerges at an oblique angle accompanied by a lifting of degeneracy, the CD for the $TE$ and $TM$ branches will have opposite sign accordingly.

# 5 Chiral transfer matrix

In the liquid crystal community, the usual approach followed for simulating transmission spectra is the Berreman matrix formalism.[S6] But this method suffers from the rise of singularities in certain specific cases.[S7] To overcome this problem, we model, in a first approximation, our polymer film under shear stress as a typical Pasteur medium, i.e. as

an isotropic chiral medium. We however introduce a spatially dispersive response of the chirality parameter of the medium in order to mimic its real response associated with extrinsic/intrinsic chirality.

In a Pasteur medium, one derives the constitutive equations as:[S8]

$$\mathbf{D} = \epsilon\mathbf{E} + i\frac{\kappa}{c}\mathbf{H} \qquad \mathbf{B} = -i\frac{\kappa}{c}\mathbf{E} + \mu\mathbf{H}, \tag{17}$$

where the permittivity ($\epsilon$), the permeability ($\mu$) and the chiral parameter ($\kappa$) are usual isotropic parameters. The source-free wave equation for such a Pasteur medium is given by:[S8]

$$\boldsymbol{\nabla}^2\mathbf{E} - i\omega\frac{\kappa}{c}\boldsymbol{\nabla}\times\mathbf{E} + i\omega(\frac{\kappa}{c}\eta\mu - \epsilon\mu)\mathbf{E} = 0. \tag{18}$$

In this case, the eigenstates are circularly polarized plane waves and the electromagnetic field inside the chiral medium can be written as a superposition of right and left polarized waves going in the forward and backward directions:

$$\begin{aligned}\mathbf{E} =& \mathbf{E}_{+R}e^{-i(\mathbf{k}_+.\mathbf{r}+\omega t)} + \mathbf{E}_{+L}e^{i(\mathbf{k}_+.\mathbf{r}-\omega t)} + \\ & \mathbf{E}_{-R}e^{-i(\mathbf{k}_-.\mathbf{r}+\omega t)} + \mathbf{E}_{-L}e^{i(\mathbf{k}_-.\mathbf{r}-\omega t)}\end{aligned}, \tag{19}$$

where $R$ and $L$ denote the right-going and left-going plane waves. These eigenstates feel the chirality of the medium as a standard medium without electromagnetic coupling, i.e.:

$$\mathbf{D}_\pm = \epsilon_\pm\mathbf{E}_\pm \qquad \mathbf{B}_\pm = \mu_\pm\mathbf{H}_\pm, \tag{20}$$

where one can derive $\epsilon_\pm$ and $\mu_\pm$ from the constitutive parameters and the wavenumber associated with each polarization state:[S8]

$$\mu_\pm = \mu \pm \frac{\kappa}{c}\sqrt{\frac{\mu}{\epsilon}} \qquad \epsilon_\pm = \epsilon \pm \frac{\kappa}{c}\sqrt{\frac{\epsilon}{\mu}} \qquad k_\pm = \omega(\sqrt{\epsilon\mu} \pm \frac{\kappa}{c}). \tag{21}$$

Our approach is similar to[S9] and to other transfer matrix computations. Once the field is characterized in the chiral medium, the field continuity equation can be written in a convenient matrix form $\mathbf{E}_{n-1} = \boldsymbol{A}_{n-1,n}\mathbf{E}_n$ where $\boldsymbol{A}$ is a bloc symmetric $4 \times 4$ matrix linking the right and left polarized electric field going forward and backward from the $(n)$ layer to the $(n-1)$ layer which are gathered in the following quadrivector $\mathbf{E}_{\mathrm{n}}$:

$$\begin{pmatrix} E_{+R} \\ E_{-R} \\ E_{+L} \\ E_{-L} \end{pmatrix}_{n-1} = \begin{pmatrix} \boldsymbol{a}_T & \boldsymbol{a}_R \\ \boldsymbol{a}_R & \boldsymbol{a}_T \end{pmatrix} \begin{pmatrix} E_{+R} \\ E_{-R} \\ E_{+L} \\ E_{-L} \end{pmatrix}_{n}, \tag{22}$$

where:

$$\boldsymbol{a}_T = \begin{pmatrix} \frac{\eta_r+1}{4}(1+\frac{cos(\theta_{+,n})}{cos(\theta_{+,n-1})}) & \frac{\eta_r-1}{4}(1-\frac{cos(\theta_{-,n})}{cos(\theta_{+,n-1})}) \\ \frac{\eta_r-1}{4}(1-\frac{cos(\theta_{+,n})}{cos(\theta_{-,n-1})}) & \frac{\eta_r+1}{4}(1+\frac{cos(\theta_{-,n-1})}{cos(\theta_{-,n-1})}) \end{pmatrix} \tag{23}$$

$$\boldsymbol{a}_R = \begin{pmatrix} \frac{\eta_r+1}{4}(1-\frac{cos(\theta_{+,n})}{cos(\theta_{+,n-1})}) & \frac{\eta_r-1}{4}(1+\frac{cos(\theta_{-,n})}{cos(\theta_{+,n-1})}) \\ \frac{\eta_r-1}{4}(1+\frac{cos(\theta_{+,n})}{cos(\theta_{-,n-1})}) & \frac{\eta_r+1}{4}(1-\frac{cos(\theta_{-,n})}{cos(\theta_{-,n-1})}) \end{pmatrix} \tag{24}$$

with $\eta_r = \frac{\eta_{n-1}}{\eta_n}$ the ratio between the usual wave impedance in their respective layer and $\theta_{\pm,n}$ the of the wave associated with the left or right polarized field that one can recover by imposing continuity of the phase at the interface, according to:

$$\theta_{\pm,n} = asin(\frac{k_{\pm,n-1}sin(\theta_\pm)}{k_{\pm,n}}). \tag{25}$$

To take into account the phase gained by the electric field inside one layer, we introduce

the $\boldsymbol{P}_n$ matrix:

$$\boldsymbol{P_n} = \begin{pmatrix} e^{-ib_+} & 0 & 0 & 0 \\ 0 & e^{-ib_-} & 0 & 0 \\ 0 & 0 & e^{ib_+} & 0 \\ 0 & 0 & 0 & e^{ib_-} \end{pmatrix} \tag{26}$$

where $b_\pm = k_{\pm,n} d_n cos(\theta_{\pm,n})$. With this, the final total transfer matrix, $\boldsymbol{T}_{tot}$, can be written as the following product of matrix:

$$\boldsymbol{T}_{tot} = \boldsymbol{A}_{0,1}\boldsymbol{P}_1\boldsymbol{A}_{1,2}...\boldsymbol{P}_N\boldsymbol{A}_{N-1,N}. \tag{27}$$

Finally, in order to measure the total field intensity transmitted by our sample, we set $E_{+L,N} = E_{-L,N} = 0$ and compute:

$$\begin{pmatrix} E_{+R} \\ E_{-R} \end{pmatrix}_{out} = \begin{pmatrix} t_{11}^{tot} & t_{12}^{tot} \\ t_{21}^{tot} & t_{22}^{tot} \end{pmatrix}^{-1} \begin{pmatrix} E_{+R} \\ E_{-R} \end{pmatrix}_{in}. \tag{28}$$

From this equation, one can easily calculate the total transmission of our sample. Moreover, probing the sample's medium with four linearly independent Stokes vectors leads to compute the MM of the sample using the chiral parameter indicated in Figure S2. In order to model this, we assume a resonance in the UV that is optically active. This resonance yields a non-zero imaginary part for the chiral parameter, which fixes the dispersive nature of our polymer, even far from the resonance through the (broad-band) Kramers-Kronig relation.

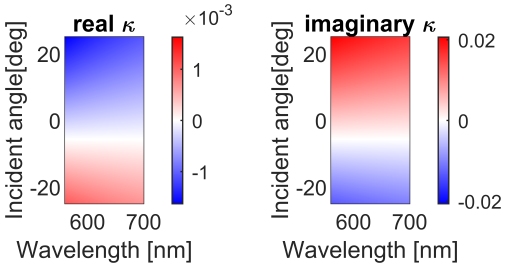


Figure S2: Real -panel (a)- and imaginary -panel (b)- parts of $\kappa_{eff}$.

Using the previously calculated matrix $\boldsymbol{A}_{n,n+1}$ and $\boldsymbol{P}_n$ and their relative $z-$positions inside the layer, one can compute the electric field intensity at any point within our multilayer system. With this, we compute the the Riemann-Silberstein vectors inside the chiral medium as defined in the main text:

$$\mathbf{G}_{\pm}(\mathbf{r}) = \mathbf{E}(\mathbf{r}) \pm i\eta\mathbf{H}(\mathbf{r}) \tag{29}$$

where $\eta$ is the usual impedance of the medium. By assuming that $\mathbf{H} = \frac{i}{\eta}\mathbf{E}$, we write:

$$\delta G(\mathbf{r}) = |\mathbf{G}_{+}(\mathbf{r})|^2 - |\mathbf{G}_{-}(\mathbf{r})|^2. \tag{30}$$

Our transfer matrix simulation allows monitoring $\delta G(\mathbf{r})$ with respect to its position along the $z-$axis for both TE and TM modes. The raw results are presented in Figure S3.

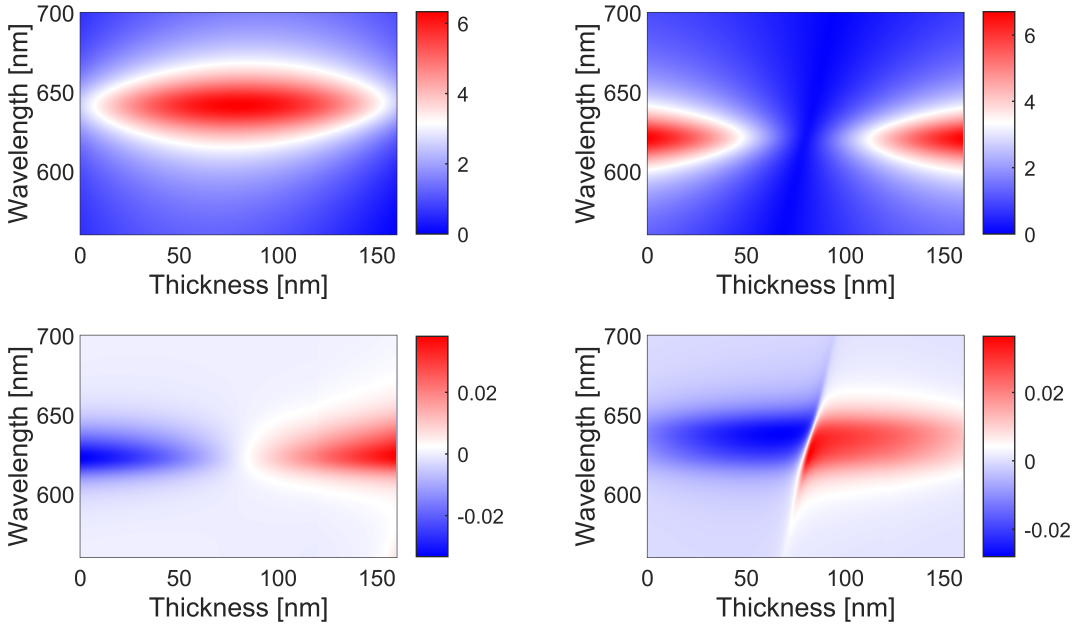


Figure S3: TE (a) and TM (b) intracavity mode electric field intensities evaluated at an angle of -25 deg ($k_{\parallel} = -5\ \mu\text{m}^{-1}$). Corresponding $\delta G_{TE}(\mathbf{r})$ (c) and $\delta G_{TM}(\mathbf{r})$ (d). The thin film boundaries are indicated with red dashed lines.

This variable leads us to monitor the local helicity of the field inside the cavity. In addition, we compute the predominant helicity of the mode by integrating along the $\hat{z}$ axis, denoting it by $\alpha_\lambda = 1/h \int_{z_1}^{z_2} \delta G(\mathbf{r}) dz$. The two simulations presented on Figure 3 (a) in the

main paper are obtained by changing the enantiomeric form associated with the extrinsic 3D chirality coming from the planar chiral structure. The value for the TE and TM modes are indicated in S4

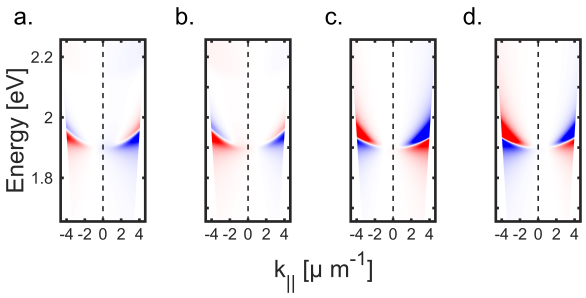


Figure S4: (a) Global helicity $\alpha_i(\lambda)$ for the $i = TE$ (a)-(b) and $i = TM$ (c)-(d) cavity mode calculated for enantiomorphic cavities with clockwise - (a)and (c)- and anticlockwise -(b)and (d)- shear stresses.

A key result is the change of the preferential helicity of the field at normal incidence as we change the enantiomeric form of the planar structure. The point where the helicity flips sign is determined by the relative strength between 2D chirality (parameter $a$ in the model) and 3D chirality (parameter $b$ in the model). In our simulations, we choosed $b/a = 10$, as discussed in the main text.

# References


(S1) Thomas, A.; Chervy, T.; Azzini, S.; Li, M.; George, J.; Genet, C.; Ebbesen, T. W. Mueller Polarimetry of Chiral Supramolecular Assembly. *J. Phys. Chem. C* **2018**, *122*, 14205–14212.

(S2) Gil, J. J. Review on Mueller matrix algebra for the analysis of polarimetric measurements. *Journal of Applied Remote Sensing* **2014**, *8*, 1 – 37.

(S3) Cloude, S. R. Conditions For The Physical Realisability Of Matrix Operators In Polarimetry. Polarization Considerations for Optical Systems II. 1990; pp 177 – 187.

(S4) Savenkov, S. N.; Grygoruk, V. I.; Muttiah, R. S.; Yushtin, K. E.; Oberemok, Y.; Yakubchak, V. V. Effective dichroism in forward scattering by inhomogeneous birefringent medium. *J. Quant. Spectrosc. Radiat. Transf.* **2009**, *110*, 30 – 42.

(S5) Arteaga, O.; Kahr, B. Characterization of homogenous depolarizing media based on Mueller matrix differential decomposition. *Opt. Lett.* **2013**, *38*, 1134–1136.

(S6) Berreman, D. W. Optics in Stratified and Anisotropic Media: 4 by 4-Matrix Formulation. *J. Opt. Soc. Am.* **1972**, *62*, 502–510.

(S7) Wu, X. The singularities in the 4 by 4 matrix formalisms. *Optik* **2018**, *168*, 10–12.

(S8) Lindell, I. V.; Sihvola, A.; Viitanen, A.; Tretyakov, S. *Electromagnetic waves in chiral and bi-isotropic media*; Artech House Publishers, 1994.

(S9) Jaggard, D. L.; Sun, X. Theory of chiral multilayers. *J. Opt. Soc. Am. A* **1992**, *9*, 804–813.